Journal of Catalysis 271 (2010) 12–21

Contents lists available at ScienceDirect

Journal of Catalysis

journal homepage: www.elsevier.com/locate/jcat

Catalytic performance and mechanism of potassium-supported Mg–Al hydrotalcite mixed oxides for soot combustion with O_2

Zhaoliang Zhang [a,*], Yexin Zhang [a,b], Zhongpeng Wang [a], Xiyan Gao [b]

[a] College of Chemistry and Chemical Engineering, University of Jinan, 106 Jiwei Rd., Jinan 250022, PR China
[b] Liaoning Key Laboratory of Internal Combustion Engines, Institute of Internal Combustion Engine, Dalian University of Technology, 2 Linggong Rd., Dalian 116024, PR China

ARTICLE INFO

Article history:
Received 1 November 2009
Revised 22 January 2010
Accepted 25 January 2010
Available online 23 February 2010

Keywords:
Soot combustion
Hydrotalcite
Potassium
Mechanism

ABSTRACT

Potassium-supported Mg–Al hydrotalcite mixed oxides were studied for soot combustion with O_2. The significant activity was elucidated by an oxygen spillover mechanism. First, the surface-activated oxygen on K sites might spill over to the free carbon sites on soot to form a carbon–oxygen complex, ketene group, which was identified as the reaction intermediate. Then the ketene group combined with another active oxygen species to give out CO_2. Two kinds of K species, Mg(Al)–O–K (tightly bound to Mg or Al) and free (isolated) K, were determined to be catalytically active sites by kinetic investigations. They could increase the reactivity and amount of surface active oxygen responsible for formation of the ketene group. The stability of K was greatly improved through the interaction with Al, which is a contribution to soot combustion of Al addition into MgO to form a K-supported composite oxide via the hydrotalcite route.

1. Introduction

In recent years, diesel engines have achieved a growing share of the light-duty vehicle market due to their high efficiency, low operating costs, high durability and reliability. However, soot particulates from these engines have caused severe environmental and health problems, meaning that their emissions must be controlled. Improvements to the technological level of the engines alone will not meet the demands of more and more stringent legislation. Suitable after-treatment technologies different from traditional three-way catalysts (TWC) are necessary. Diesel particulate filters (DPF), which can trap over 90% of soot and be regenerated by combustion of collected soot, seem to be most promising [1]. Unfortunately, the combustion temperature of soot (above 450 °C) is beyond the normal diesel exhaust temperature range (175–400 °C). To accomplish the regeneration of DPF at lower temperatures, various catalysts, such as noble metals [2], transition metals [3,4], perovskites [5], spinels [6], earth alkali metals [7] and alkali metals [8], have been developed to decrease soot ignition temperature. Therein, potassium-containing materials have attracted increasing interest as potassium (K) shows better promotion of catalytic activity than other alkali elements for soot combustion [1]. Nevertheless, the proposed roles of K vary, and the relevant mechanisms for soot combustion are still being debated. Serra et al. [9] assessed a Cu–K–V catalyst for soot combustion and found that the presence of liquid eutectic phases of K dramatically improves the catalyst–soot contact, constituting a key factor in determining the catalytic activity. Contrarily, Miró et al. [10], in the investigation into K-supported MgO and CeO_2, proposed a mechanism involving surface carbonate species, in which K aids soot combustion by consuming the carbon to form carbonate intermediates. Comparatively, more investigations have explained the role of K in term of redox mechanism. Jiménez et al. [11] showed K facilitates the formation and migration of oxygen species by weakening the bonds between metals and oxygen, and Janiak et al. [12] revealed that K can enhance the sticking and dissociation of gas phase O_2 as an electron donor; a similar view was presented by Jiménez et al. [7]. It is worthy to note that Aneggi et al. [8] suggested a carbon–oxygen complex mechanism for ceria promoted with alkali metals, in which surface carbonate species were active sites. However, the types of carbonate species were not proposed and proven because of the restriction of temperature-programmed reduction (TPR) technique they adopted. Recently, Gross et al. [13] observed the kinetic evidence related to carbonate mechanism of soot combustion on K/CeO_2, which suggests that the kinetics is a good way to study the role of K in soot combustion. On the other hand, the stability of K on catalysts is still a great challenge though many effects have been made [14].

For several years, Mg–Al hydrotalcite mixed oxides were reported to offer potential advantages over Pt/BaO/Al_2O_3 in NO_x (another important pollutant from diesel exhaust) storage-reduction (NSR) and assessed to be the new generation of NSR catalysts [15,16]. In previous research [17], we also displayed improved

* Corresponding author. Fax: +86 531 89736032.
E-mail address: chm_zhangzl@ujn.edu.cn (Z. Zhang).

0021-9517/$ - see front matter © 2010 Elsevier Inc. All rights reserved.
doi:10.1016/j.jcat.2010.01.022

activity by the addition of K for soot combustion. The promotion effect of K was preliminarily interpreted as an interaction between K and Mg (Al), which might weaken the Mg(Al)–O band, thus facilitating the mobility of the oxygen species. However, this initial hypothesis was not borne out by experimental evidence. In the present work, K_2CO_3-supported Mg–Al hydrotalcite mixed oxides for soot combustion with O_2 were studied in depth by X-ray powder diffraction (XRD), X-ray fluorescence (XRF), N_2 adsorption/desorption, differential scanning calorimetry (DSC), TPR, diffuse reflectance infrared Fourier transform (DRIFT) spectroscopy, temperature-programmed desorption (TPD), X-ray photoelectron spectroscopy (XPS), Fourier transform infrared (FTIR) spectroscopy, temperature-programmed oxidation (TPO), carbothermal reduction, isothermal and transient reactions. Considering these results, we have proposed a probable reaction mechanism based on turnover frequency and found that the stability of K was greatly improved through the interaction with Al.

2. Experimental

2.1. Sample preparation

The Mg–Al hydrotalcite with molar ratio of 3:1 was prepared by co-precipitation from aqueous solutions of $Mg(NO_3)_2{\cdot}6H_2O$ and $Al(NO_3)_3{\cdot}9H_2O$ at a constant pH of 10. The mixture of metal nitrates was contacted with a basic solution of Na_2CO_3 and NaOH by dropwise addition of both solutions into a stirred beaker containing 200 mL of deionized water held at 65 °C. The resulting precipitates were kept in suspension at 65 °C for 30 min under stirring, then were filtered, thoroughly washed with distilled water and dried overnight at 120 °C. The prepared hydrotalcite was calcined at 950 °C for 12 h, and the mixed oxide of MgAlO and $MgAl_2O_4$ (spinel) was obtained (see the inset in Fig. 3a). For comparison, MgO was prepared by precipitation of $Mg(NO_3)_2{\cdot}6H_2O$ using ammonia and calcination at 950 °C for 12 h, while Al_2O_3 was obtained by calcination of boehmite (AlOOH) at 950 °C for 12 h.

The K-supported samples were prepared by impregnation method using K_2CO_3 as a precursor. The mixed oxide suspension in the aqueous solution of K_2CO_3 was evaporated while being stirred at 90 °C until achieving a paste, which was then dried at 120 °C overnight and calcined at 850 °C for 2 h. In this way, catalysts containing 2, 5, 8 and 15 wt.% of K were prepared and denoted as 2K/MgAlO, 5K/MgAlO, 8K/MgAlO and 15K/MgAlO, respectively. For comparison, a K-free sample was also prepared with the same procedure except for the addition of K_2CO_3 and was named 0K/MgAlO. The K-supported pure oxides of MgO and Al_2O_3 were prepared with 8 wt.% of K and denoted as 8K/MgO and 8K/Al_2O_3, respectively.

2.2. Catalytic reactions

The model soot used in this study was Printex-U from Degussa with a Brunauer–Emmett–Teller (BET) surface area of 93.5 m^2/g. Elemental analysis showed its carbonaceous nature with 90.43 wt.% C, 1.09 wt.% H, 0.17 wt.% N and 0.51 wt.% S. The volatile matter is detected to be about 5 wt.% and desorbed at about 200 °C (by thermogravimetry). The mean agglomerate size measured using a Beckman Counter LS13320 laser particle size analyzer was about 177 nm. The catalytic reactions for soot combustion were performed by a TPO technique in a fixed-bed flow reactor. The soot/catalyst weight ratio was 1:9. Two types of contact between soot and catalyst were used [18]: tight contact was attained by grinding soot with catalyst in an agate mortar for 30 min and palletizing for 10 min under the pressure of 20 MPa, and then crushing and sieving to 20–60 mesh; loose contact was achieved by grinding soot and catalyst separately and shaking the mixtures in a sample bottle for 24 h.

Typically, a 50 mg sample of the soot/catalyst mixture was pretreated in a flow of He (50 ml/min) at 200 °C for 1 h to remove surface-adsorbed species. After cooling down to room temperature, a gas flow with 9.97% oxygen in He (100 ml/min) was introduced and then TPO was started at a heating rate of 5 °C/min until 800 °C. The concentrations of CO_2 and CO in the effluent were online analyzed by a gas chromatograph (GC) (SP-6890, Shandong Lunan Ruihong Chemical Instrument Corporation, China) with a flame ionization detector (FID) after separating them over a Porapak Q column and converting to methane over a Ni catalyst at 360 °C. From the TPO results, two parameters were derived in order to evaluate the catalytic performance: one was the temperature corresponding to the maximum soot combustion rate (T_m), and the other was the selectivity to CO_2 formation (S_{CO_2}), which was defined as the produced CO_2 amount divided by the total amounts of CO_2 and CO. The lower the T_m value and the higher the S_{CO_2} value, the more active the catalyst. In addition, the sensitivity of the catalysts to physical contact can be assessed through the value of ΔT_m, defined as $\Delta T_m = T_m$ (loose contact) $- T_m$ (tight contact) [20].

The isothermal reactions for soot combustion were also conducted, at which a stable and small conversion of soot (1–2%) was achieved in an approximate kinetic regime. Thus, the reaction rate, turnover frequency (TOF) and apparent activation energy (E_a) of soot combustion can be obtained [21]. Therein, TOF_K is on the basis of K-supporting amount. As K dispersion might be determined by CO_2 chemisorption at 250 °C [22,23], TOF_{CO_2}, which is on the basis of active K sites, could be calculated assuming that one CO_2 molecule adsorbs on one K_2O site to form the surface carbonate.

2.3. Catalyst characterization

The chemical compositions of catalysts before and after reactions were measured by XRF (ARL9400, Switzerland).

XRD patterns were recorded on a Rigaku D/max-rc diffractometer employing Cu Kα radiation.

N_2 adsorption/desorption was measured by a Micromeritics ASAP 2020 surface area analyzer after outgassing at 300 °C for 5 h prior to analysis. The specific surface areas were calculated with the BET equation. The pore size distributions were obtained by the Barrett–Joyner–Halenda (BJH) methods using the desorption branch of the isotherms.

CO-TPR was conducted in a fixed-bed flow reactor. A 50 mg sample was heated in a flow of high purity O_2 (20 ml/min) at 500 °C for 1 h. After cooling down to room temperature, the CO-TPR test was carried out in the flow of 4007 ppm CO in He (50 ml/min) at a heating rate of 10 °C/min. CO and CO_2 concentrations in the effluent gas were online monitored using a GC.

In situ DRIFT spectra of CO adsorption was performed on a Bruker Tensor 27 spectrometer equipped with a mercury–cadmium–telluride (MCT) detector. Prior to the measurements, the sample was treated *in situ* at 400 °C in He (30 ml/min), and subsequently cooled down to 50 °C. During the cooling stage, the background spectra of the treated samples were taken at desired temperatures. The flow was then switched to a gas mixture of 4007 ppm CO in He (30 ml/min). Finally, the spectra were collected at targeted temperatures, accumulating 64 scans at a resolution of 4 cm^{-1} and displayed in Kubelka–Munk units.

CO_2-TPD was carried out in a fixed-bed flow reactor. A 50 mg sample was pretreated in He at 500 °C for 1 h. After cooling down to 50 °C, 4058 ppm CO_2 was introduced and adsorbed until saturation. Desorption was started at a heating rate of 10 °C/min in He (50 ml/min). The desorbed CO_2 and H_2O were detected by GC

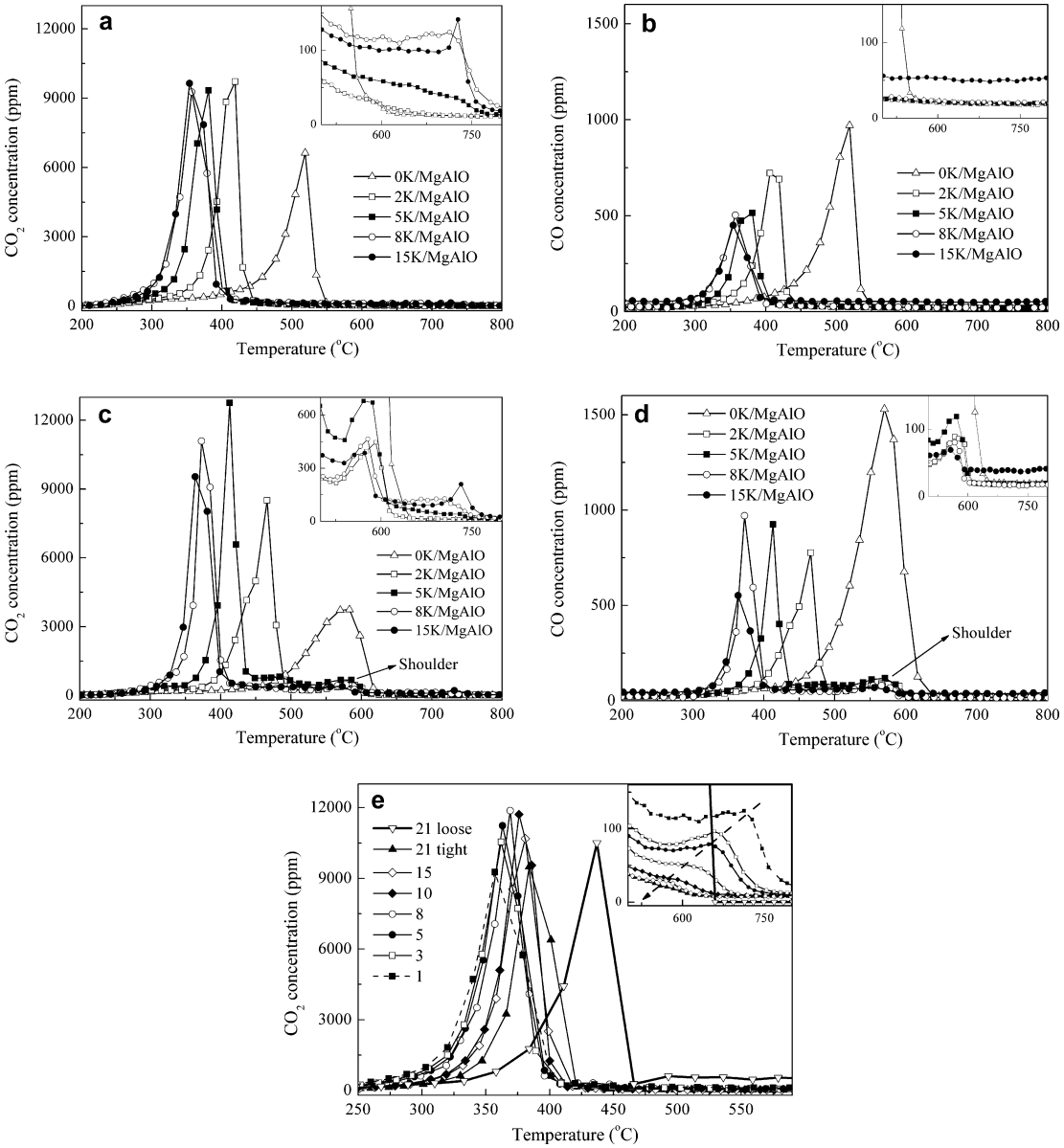

Fig. 1. TPO patterns of CO_2 (a and c) and CO (b and d) for soot combustion on catalysts under tight (a and b) and loose (c and d) contact conditions. (e) Repeated TPO patterns of CO_2 for soot combustion on the 8K/MgAlO sample under tight contact condition.

Table 1
The texture properties and catalytic activity of soot combustion on samples.

Samples	BET surface area (m^2/g)	Pore volume (cm^3/g)	E_a (kJ/mol)	TOF_K at 260 °C ($s^{-1} \times 10^{-5}$)	T_m (°C)		ΔT	S_{CO_2} (%)	
					Tight	Loose		Tight	Loose
0K/MgAlO	116.1	0.26	–	–	519	583	64	87.9	75.7
2K/MgAlO	88.9	0.21	110.1	6.05	419	466	47	92.7	91.7
5K/MgAlO	72.7	0.18	112.6	5.69	381	413	32	94.9	93.1
8K/MgAlO	46.6	0.12	110.2	3.97	357 (384)[a]	373 (437)[a]	16 (53)[a]	95.4 (95.7)[a]	93.4 (97.4)[a]
15K/MgAlO	13.2	0.10	–	–	354	364	10	97.0	95.5
8K/MgO	22.3	0.04	–	–	351 (434)[a]	–	–	97.0 (93.2)[a]	–
8K/Al_2O_3	63.7	0.28	–	–	377 (428)[a]	–	–	96.4 (94.4)[a]	–

[a] Twenty-one times TPO.

and quadruple mass spectrometer (MS, OmniStar 200, Balzers), respectively.

XPS data were taken on an AXIS-Ultra instrument from Kratos Analytical using monochromatic Al Kα radiation (225 W, 15 mA, 15 kV) and low-energy electron flooding for charge compensation. To compensate for surface charges effects, binding energies were calibrated using C 1s hydrocarbon peak at 284.80 eV.

The partially oxidized soot–8K/MgAlO sample was obtained by quenching the TPO reaction of the soot and 8K/MgAlO mixture under tight contact at 350 °C (T_m). The FTIR spectrum of the sample was recorded on a Bruker Tensor 27 spectrometer in the range of 400–4000 cm^{-1} using the KBr dilution. For comparison, FTIR spectra of the fresh soot–8K/MgAlO mixture under tight contact and the used 8K/MgAlO sample after TPO were also recorded.

Carbothermal reduction in the absence of gas phase oxygen was done in a fixed-bed flow reactor. A 50 mg sample of the soot/catalyst mixture (1:9, weight ratio) under tight contact was pretreated in He (100 ml/min) at 200 °C for 1 h and then heated at 5 °C/min from room temperature to 900 °C.

The transient reaction was performed in a fixed-bed flow reactor. Prior to the reaction, a 50 mg sample of the soot and 8K/MgAlO mixture under tight contact was pretreated in He (50 ml/min) at 200 °C for 1 h. The transient reaction was then started and separated into three phases. In the 1st phase, a TPO reaction was carried out with 9.97% oxygen in He (100 ml/min) at a heating rate of 5 °C/min up to 350 °C. Then the 2nd phase was started by switching to the flow of He (50 ml/min), and the sample was flushed for 1 h at 350 °C. In the final phase, the mixture was further heated to 900 °C at a rate of 5 °C /min.

3. Results

3.1. TPO and isothermal reactions

Fig. 1 shows the TPO patterns of soot combustion on catalysts under both tight and loose contact conditions. The derived values of T_m, S_{CO_2} and ΔT_m are summarized in Table 1. T_m and S_{CO_2} for the uncatalyzed soot combustion were about 613 °C and 69.3%, respectively. The 0K/MgAlO sample shows modest activity only in tight contact condition, but all TPO patterns for both tight and loose contacts shift to lower temperatures after K addition. Furthermore, T_m and ΔT_m decreased, while S_{CO_2} slightly increased monotonously with the increase in K amounts. These results indicated that the presence of K significantly improved the activity and the selectivity to CO_2 and depressed the sensitivity to contact between soot and catalyst. Because the 15K/MgAlO sample shows nearly the same T_m as the 8K/MgAlO sample, further increase in K amount is unnecessary in terms of T_m, which suggests the supporting amount of K should not be more than 8 wt.%. This is consistent with the optimum K content about 7 wt.% for Ba,K/CeO_2 [19].

Under tight contact conditions, one CO_x peak was observed for all samples, while a main peak and a shoulder (~575 °C) were observed for K-supported samples under loose contact conditions. The shoulder peak was attributed to uncatalyzed combustion due to poor contact between soot and catalyst. Furthermore, as shown in the insets in Fig. 1a and c, a weak CO_2 desorption peak after soot combustion completion was also found in the 8K/MgAlO and 15K/MgAlO samples at 700–750 °C under both tight and loose contact conditions; this is not the case, however, for CO (insets in Fig. 1b and d).

Fig. 1e shows the repeated TPO patterns of the 8K/MgAlO sample. Although the selectivity to CO_2 was more or less the same, after 20 cycles of TPO, T_m rose about 7% and 15% under tight and loose contact, respectively. This rise corresponds to the gradual disappearance of the weak peak of CO_2 at 700–750 °C. Simultaneously, ΔT_m rose to the value near to that of 2K/MgAlO.

As shown in Fig. 2, E_a and TOF_K at 260 °C were calculated and given in Table 1. TOF_K decreased in the sequence of 2K/MgAlO > 5K/MgAlO > 8K/MgAlO, suggesting the specific catalytic activ-

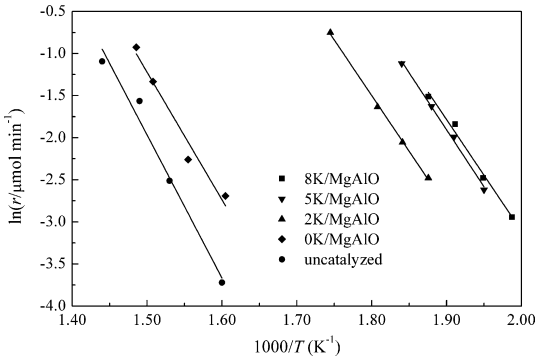

Fig. 2. Arrhenius plots for uncatalyzed and catalyzed soot combustion.

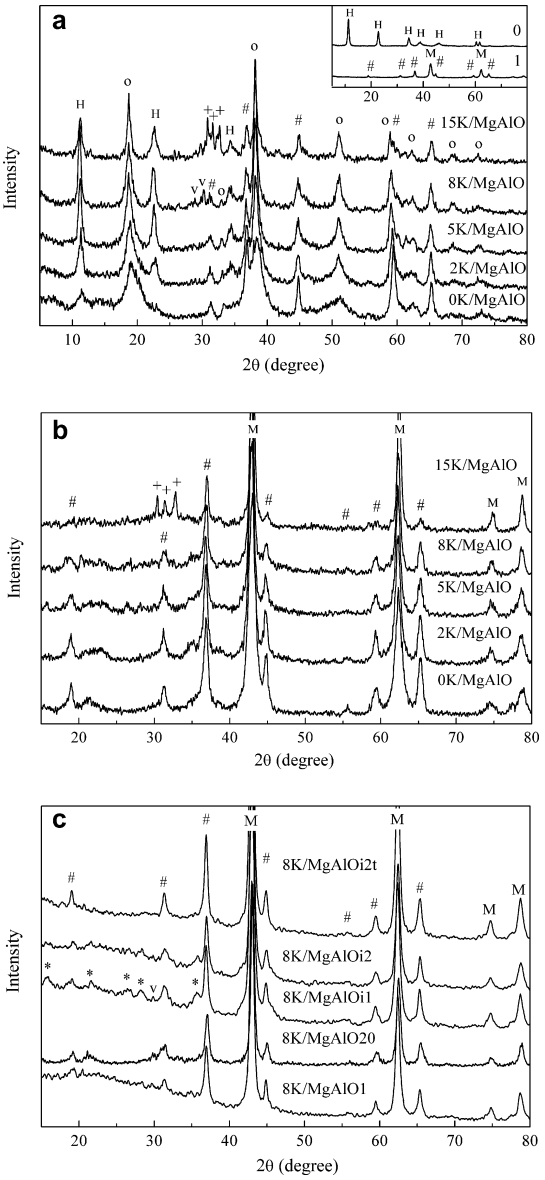

Fig. 3. XRD patterns of the 0K/MgAlO, 2K/MgAlO, 5K/MgAlO, 8K/MgAlO and 15K/MgAlO samples before (a) and after (b) calcination as well as the 8K/MgAlO sample after reactions (c). 8K/MgAlO1: after 1 time TPO reaction; 8K/MgAlO20: after 20 times TPO reactions; 8K/MgAlOi1: after isothermal combustion at 350 °C with soot/catalyst = 1/2; 8K/MgAlOi2: after isothermal combustion at 350 °C with soot/catalyst = 1/4; and 8K/MgAlOi2t: after TPD of the 8K/MgAlOi2 sample in He until 800 °C. The insets in (a) are the patters of Mg–Al hydrotalcite (1) and its derived oxides (2). H: hydrotalcite; o: $Mg(OH)_2$; M: MgO; #: $MgAl_2O_4$; +: K_2CO_3; v: $K_2Mg(CO_3)_2{\cdot}4H_2O$; ∗: $KAl(CO_3)(OH)_2$.

ity is contrary to what is shown by T_m. E_a for the uncatalyzed reaction is around 141 kJ/mol, which decreased to about 110 kJ/mol for K-supported MgAlO. This suggests that the reaction mechanism might be changed in the presence of K-supported MgAlO catalysts.

3.2. Characterization

3.2.1. XRD

Fig. 3 shows the XRD patterns of the hydrotalcite-derived samples after supporting K_2CO_3. In the inset of Fig. 3a, Mg–Al hydrotalcite structure (JCPDS 70-2151) was confirmed (Fig. 3a0). The derived oxide consists of ill-crystalline periclase MgO (JCPDS 45-0946) and spinel-type $MgAl_2O_4$ (JCPDS 21-1152) phases (Fig. 3a1). After the mixed oxide was rehydrated with water or supported with K_2CO_3, the MgO phase would convert into brucite $Mg(OH)_2$ (JCPDS 86-0441) and the hydrotalcite structure partially recovered. All K-supported samples show stronger (0 0 3) and (0 0 6) peaks than the 0K/MgAlO sample, suggesting that K salt enhances the recovery of the hydrotalcite structure. Furthermore, as the amount of K increased to 8 wt.%, a new phase $K_2Mg(CO_3)_2{\cdot}4H_2O$ (JCPDS 83-1955) appeared. It has been found that, when the supporting amount approaches the monolayer dispersion threshold, the interaction between K_2CO_3 and the support becomes so strong as to lead to formation of such a stoichiometric substance [24]. This suggests that the highest limit of the monolayer dispersion of K^+ ions on hydrotalcite-derived oxide is not more than 8 wt.% of the supporting amount. However, only in the 15K/MgAlO sample can the K_2CO_3 (JCPDS 49-1093) phase be observed.

Fig. 3b shows the XRD patterns of the above samples after calcination at 850 °C for 2 h. While the crystalline K_2CO_3 still remained on the 15K/MgAlO sample, the 2K/MgAlO, 5K/MgAlO and 8K/MgAlO samples show only MgO and $MgAl_2O_4$ phases, similar to the 0K/MgAlO sample, which implies the high dispersion of K species on the surface. This is reasonable because the low-temperature decomposition of supported K_2CO_3 was reported to occur via interactions with surface hydroxy groups [25]. In addition, $K_2Mg(CO_3)_2{\cdot}4H_2O$ was said to decompose into K_2CO_3 at 350–400 °C [26], which can be further decomposed into KO_x species and CO_2 [27]. This is also demonstrated by the temperature-programmed decomposition profile of the 8K/MgAlO sample before calcination, which presents CO_2 desorption at 700–850 °C (results not shown here).

Taking the 8K/MgAlO sample as an example, Fig. 3c shows the XRD patterns of the used catalysts. After 1–20 times TPO cycles, the 8K/MgAlO sample retained its original state. In addition, the $K_2Mg(CO_3)_2{\cdot}4H_2O$ phase was likely formed due to air exposure. However, both 8K/MgAlOi1 and 8K/MgAlOi2 samples show $K_2Mg(CO_3)_2{\cdot}4H_2O$ and a new phase, $KAl(CO_3)(OH)_2$ (JCPDS 21-0979), which confirms the formation of Mg–O–K and Al–O–K bonds on K-supported samples. $KAl(CO_3)(OH)_2$ was reported to decompose into aluminates and/or high dispersions of surface K bound to Al at about 320 °C (the optimum decomposition temperature is 420 °C), depending on K amount and calcination temperatures [25,27]. As no aluminates were detected on the 8K/MgAlOi2t sample, the latter was expected.

3.2.2. Textural property (BET and pore distribution)

Table 1 also shows the BET surface areas and pore volumes of samples. A monotonous decrease was observed for both with the increase in K amount, which corresponds to the increase in pore sizes. This suggests that the supported K species blocked some pores and caused dense surface coverage, especially for the 15K/MgAlO sample that presented bulk K_2CO_3 phase.

3.2.3. In situ DRIFT spectra of CO adsorption

Fig. 4 shows *in situ* DRIFT spectra of CO adsorption on the 0K/MgAlO, 5K/MgAlO and 8K/MgAlO samples. The assignments of some IR bands are summarized in Table 2. As shown in Fig. 4A, the 8K/MgAlO sample always exhibits a strong doublet assigned to physisorbed CO_2 at 2361 and 2343 cm^{-1}, which intensified when heated to 200 °C and weakened at 250 °C. In the case of the 5K/MgAlO sample, the same doublet was raised at 100 °C but was much weaker. No relevant bands were detected on the 0K/MgAlO sample.

For both K-supported samples, some pronounced bands assigned to carboxy species were detected between 1200 and 1800 cm^{-1}. The formate was formed at a lower temperature and transformed into carboxylate at 150 °C, which then intensified at 200 °C. When the temperature reached 250 °C, some carboxylates developed into carbonates. This was not the case for 0K/MgAlO, in which these signals are very weak.

The above two occurrences suggest that CO can be more easily oxidized into CO_2 rather than carbonates on the K-supported samples. This was assigned to the formation of surface suprafacial, weakly chemisorbed oxygen (for instance, O_2^-), after K addition. Be-

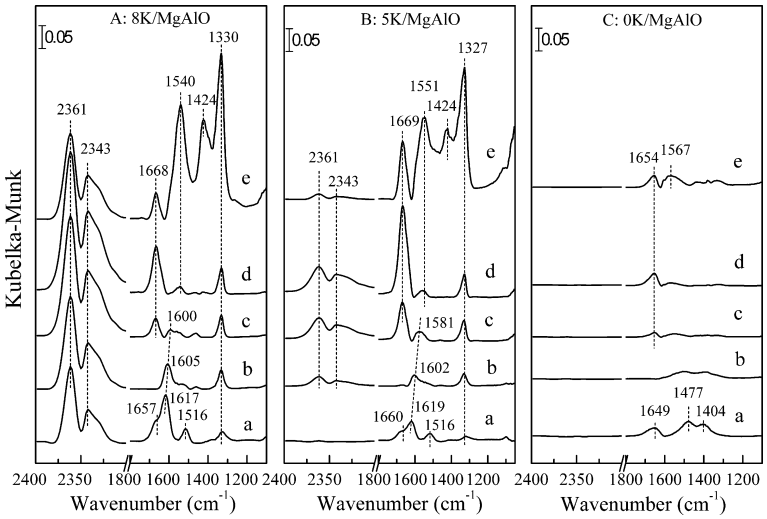

Fig. 4. *In situ* DRIFT spectra of CO adsorption on the 8K/MgAlO (A), 5K/MgAlO (B) and 0K/MgAlO (C) samples at 50 °C (a), 100 °C (b), 150 °C (c), 200 °C (d) and 250 °C (e).

Table 2
IR bands and assignments of the species formed after CO adsorption on samples.

IR bands (cm^{-1})	Assignments	Samples	Ref.
2361, 2343	Physisorbed CO_2	5, 8K/MgAlO	[28]
1670–1650	Carboxylate	0, 5, 8K/MgAlO	[29,30]
1615–1600	Formate	5, 8K/MgAlO	[29,31]
1550–1510, 1330–1325	Monodentate carbonate	5, 8K/MgAlO	[29]
1424	Carbonate bridging K^+ and Al^{3+} ions	5, 8K/MgAlO	[25,32]
1649, 1477	Bicarbonate	0K/MgAlO	[33]
1404	Carbonate bonding to Mg	0K/MgAlO	[34]
1660–1650	H_2O	0, 5, 8K/MgAlO	[32]

cause of the lower electro-negativity of K, the greater ease of electron release resulted in the weakening of the K–O bond [11]. Furthermore, the formed CO_2 is easily desorbed at soot ignition temperature.

3.2.4. CO-TPR

Fig. 5 shows the consumption of CO and the resulting production of CO_2 as well as CO_x concentrations during CO-TPR, which confirmed the above DRIFT results. All K-supported samples show lower ignition temperatures and larger amounts of CO consumption compared with the 0K/MgAlO sample. This suggests a great increase in the reactivity and amount of active oxygen, as indicated in Section 3.2.3. An increase in the K-supporting amount from 2 to 8 wt.% progressively shifted the TPR plots to lower temperatures. In addition, as seen from CO_x curves, an additional CO_2 desorption peak at 700–800 °C for the K-supported samples was also observed, which is evidently not from the direct oxidation of CO by catalysts. The more the K amount, the stronger the peak is. Compared with the insets in Fig. 1a, c and e, it accords with the weak CO_2 peak at 700–750 °C in TPO patterns.

3.2.5. CO_2-TPD

Fig. 6a shows the CO_2-TPD profiles of 0K/MgAlO, 2K/MgAlO, 5K/MgAlO, 8K/MgAlO and 8K/MgAlO20 samples. The simultaneous desorption of H_2O was also monitored by MS for reference. The inset for 8K/MgAlOi2t was done as follows: as soon as the 8K/MgAlO sample completed isothermal soot combustion (soot/catalyst = 1/4) at 350 °C and cooled down to room temperature in He, the temperature-programmed decomposition was proceeded in the same condition as that used in CO_2-TPD. The 0K/MgAlO sample shows a wide spectrum from room temperature to about 450 °C, which was deconvoluted by Di Cosimo et al. [35] into three CO_2 adsorbed species: bicarbonates on weakly basic OH groups, bidentate carbonates on Mg–O pairs with accessible cations and unidentate carbonates on strongly basic surface O^{2-} anions. As to the K-supported samples, CO_2 desorption peaks at lower temperatures shift toward to higher temperatures, which might be caused by the changes in adsorption species. Furthermore, the peak displayed much more CO_2 desorption for the 5K/MgAlO and 8K/MgAlO samples. As noted earlier, the two phenomena could be attributed to the CO_2 adsorption on Mg–O–K and Al–O–K basic sites (for instance, the formation of adsorbed $K_2Mg(CO_3)_2$ and $KAl(CO_3)(OH)_2$ species). Importantly, a wide CO_2 desorption above 450 °C was observed, which can be exclusively correlated with new sites caused by the addition of K. The peak, which corresponds to the CO_2 peak at higher temperatures in TPO and CO-TPR, also appeared on 8K/MgAlOi2t at about 725 °C. These new sites are likely, for instance, strong basic sites and/or sites for formation of carbonates such as K_2CO_3.

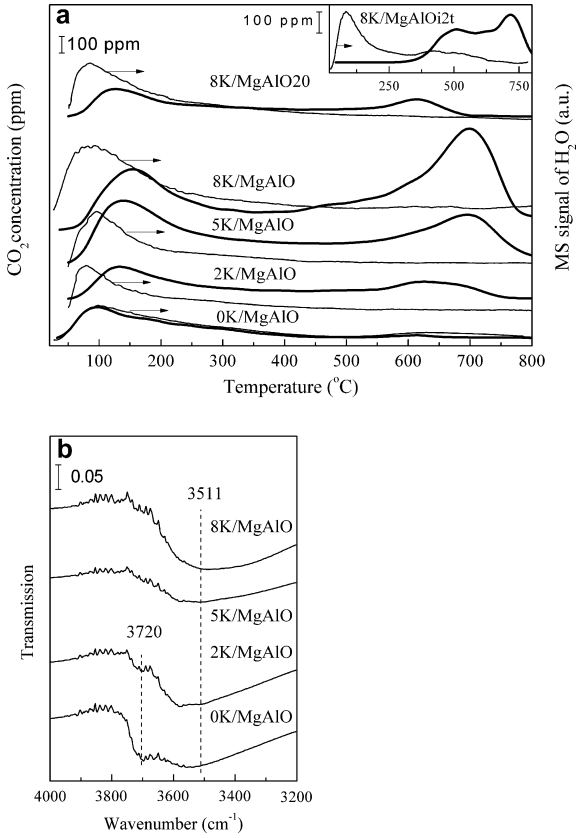

Fig. 6. (a) CO_2-TPD profiles of the 0K/MgAlO, 2K/MgAlO, 5K/MgAlO, 8K/MgAlO and 8K/MgAlO20 samples at 50 °C. The inset is for 8K/MgAlOi2 (see text). (b) *In situ* FTIR spectra of the 0K/MgAlO, 2K/MgAlO, 5K/MgAlO and 8K/MgAlO samples at 250 °C after heat treatment at 500 °C for 1 h in He.

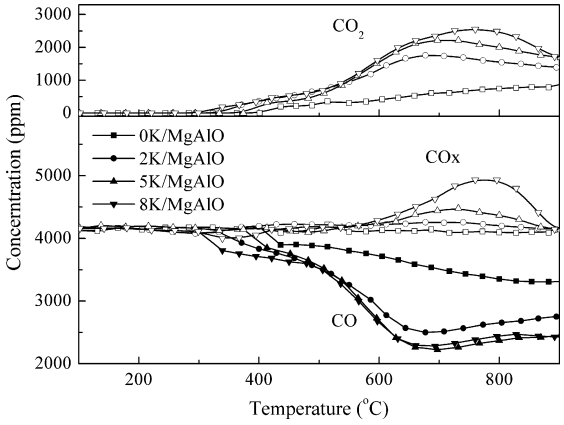

Fig. 5. CO-TPR profiles of the 0K/MgAlO, 2K/MgAlO, 5K/MgAlO and 8K/MgAlO samples. CO_x: the sum of CO_2 and CO concentrations.

For the purpose of removal of physisorption and bicarbonates, CO_2 adsorption at 250 °C was also conducted. The ratio of CO_2/

K_2O was listed in Table 3. The high ratio for the 2K/MgAlO sample, together with the high TOF_K, is thus interpreted as evidence for the highest K dispersion. On the other hand, the low ratio for the 5K/MgAlO and 8K/MgAlO samples suggests a low K dispersion. Therefore, combined with XRD results, two kinds of K species were thus expected at least on samples with high supporting amount of K [23]. One K species (K_I) had better contacts and strong interaction with supports in relatively small particle sizes, which were highly dispersed and most probably formed through the replacement of the hydroxyl groups on calcined hydrotalcite by K^+ ions as confirmed by ^1H MAS NMR [24]. Our results of the *in situ* FTIR spectra at 250 °C also confirmed this. As shown in Fig. 6b, the hydrogen-bonded hydroxy groups at 3511 cm^{-1} were found on the 0K/MgAlO and K-supported samples, while the band due to isolated hydroxy groups (Mg(Al)–OH) at 3720 cm^{-1} diminished for the 2K/MgAlO sample and vanished for the 5K/MgAlO and 8K/MgAlO samples, which should be related to the suggested conversion of Mg(Al)–OH into Mg(Al)–OK surface groups [25]. These K species were shown by the lower temperature of CO_2 desorption at higher temperature for the 2K/MgAlO sample compared to the 5K/MgAlO and 8K/MgAlO samples. Another K species (K_{II}) could be the free (isolated) K (including bulk K_2CO_3 for 15K/MgAlO), which were in larger particle sizes [22]. These K species were more easily lost (for instance, through sublimation [1]), as shown by the amount of CO_2 desorption at higher temperatures, which decreased greatly for the 8K/MgAlO20 sample compared to the 8K/MgAlO sample.

The strong correlation of the ratio of CO_2/K_2O and TOF_K suggests that the reaction proceeds mainly on the K sites. In order to judge whether this was accurate, TOF_{CO_2} at 260 °C was calculated. As shown in Table 3, no significant difference in the TOF_{CO_2} on K-supported catalysts was observed irrespective of different supporting amounts of K, which clearly indicates that the reaction proceeds mainly on the K sites [36]. This finding was also reported in a previous study by An and McGinn [1].

3.2.6. XPS

Fig. 7 shows XPS spectra of O 1s, C 1s and K 2p for the 0K/MgAlO, 8K/MgAlO and 8K/MgAlO20 samples. The surface concentrations (expressed as percentage of surface atomic ratios) are presented in Table 4. The broad O 1s spectra were observed for all samples. Peak deconvolution and fitting reveal the samples are comprised of two well-defined components, O_I and O_{II}, representing two different kinds of surface species. It is generally agreed that O_I, with lower binding energy (BE) (~530 eV), is characteristic of the lattice oxygen bound to metal cations of the structure [37], while O_{II}, with a higher BE (~531 eV), belongs most likely to surface oxygen such as hydroxyl and carbonate oxygen [10,37]. The O 1s peak of 8K/MgAlO shifts to a lower BE compared with 0K/MgAlO, which can be related basically to the elimination of hydroxyl groups simultaneous to the decomposition of surface carbonates [25]. In the C ls region, two peaks are detected. The C_I peak at 284.8 eV does not change in position and is likely associated with carbon contaminations. The second peak C_{II} at ~289.4 eV is mostly likely due to carbonate carbon. The lowest C_{II} value for 8K/MgAlO leads us to infer that the supported K_2CO_3 has decomposed after calcination. These modifications might suggest that the 8K/MgAlO sample possessed more lattice oxygen than the 0K/MgAlO sample, as shown in Table 4. After 20 times TPO, the concentrations of these surface lattice oxygen species decreased, confirming their suitability for soot combustion [10]. The atomic ratio of Mg/Al on the 0K/MgAlO sample was about 2.27, a little lower than the stoichiometry. For the 8K/MgAlO sample, this ratio dropped further, suggesting that the surface is rich in Al for fresh samples. Such surface enrichment of Al upon calcination has also been observed in many studies [38]. However, in comparison with 8K/MgAlO, the 8K/MgAlO20 sample shows a large reduction in K (the peak intensity of K 2p in Fig. 8b weakened) and Al concentrations simultaneously, while Mg and C (C_{II}) concentrations increased.

Table 3
CO_2 adsorption at 250 °C and TOF_{CO_2}.

Samples	CO_2 adsorbed at 250 °C (μmol/g)	CO_2/K_2O	TOF_{CO_2} at 260 °C ($s^{-1} \times 10^{-3}$)
2K/MgAlO	44.15	0.17	1.41
5K/MgAlO	91.09	0.14	1.60
8K/MgAlO	101.52	0.10	1.61

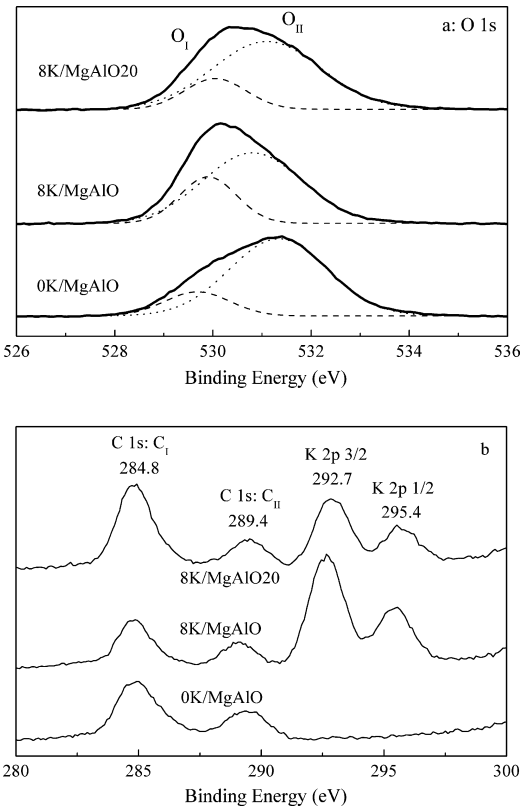

Fig. 7. XPS spectra of O 1s (a), C 1s and K 2p (b) for the 0K/MgAlO, 8K/MgAlO and 8K/MgAlO20 samples.

3.2.7. Ex situ FTIR

In order to investigate the intermediate species on K-supported catalysts for soot combustion, the FTIR spectra of partly oxidized soot–8K/MgAlO and soot–0K/MgAlO samples were recorded *ex situ* and compared with the spectra of the nonoxidized and fully oxidized samples. As shown in Fig. 8, no marked difference is shown between the nonoxidized and fully oxidized samples. In the case of partly oxidized mixture, a well-defined band at 2171 cm^{-1} was observed, which is the characteristic bond of the ketene group arising from out-of-phase or antisymmetric stretch of the C=C=O moiety [39,40]. However, the ketene group was not seen in the soot–0K/MgAlO sample (results not shown here). This suggests that K is prerequisite to the formation of the ketene group, a carbon–oxygen complex formed during soot combustion for K-supported samples.

3.3. Carbothermal reduction

Carbothermal reduction under the flow of high purity He was thought to give information on intrinsic oxidation capability. As

Table 4
XPS analysis results.

Samples	Surface atomic ratio (%)					Mg/Al	K/(Mg + Al)
	Mg	Al	K	O (O_I)[a]	C (C_{II})[b]		
0K/MgAlO	20.03	8.81	–	55.65 (9.75)	15.52 (7.34)	2.27 (3)[c]	–
8K/MgAlO	16.86	15.09	3.94	55.62 (15.18)	8.50 (2.79)	1.12	0.12
8K/MgAlO20	18.68	11.98	2.28	52.53 (10.80)	14.53 (3.92)	1.56	0.07

[a] Surface lattice oxygen.
[b] Carbon due exclusively to the C 1s (289.4 eV) species.
[c] Bulk ratio based on stoichiometry.

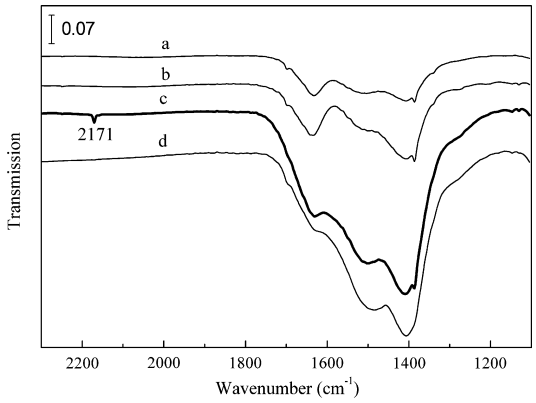

Fig. 8. *Ex situ* FTIR spectra of the nonoxidized soot–8K/MgAlO mixture (1/9 weight ratio) under tight contact (a), the fully oxidized mixture after TPO test (b), the partly oxidized mixture obtained by stopping the TPO test at 350 °C (c), and the mixture at the end of 2nd phase in transient reaction (d), see text.

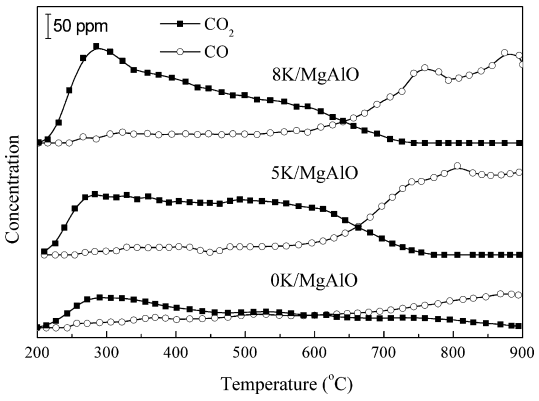

Fig. 9. Carbothermic reduction of soot on the 0K/MgAlO, 5K/MgAlO and 8K/MgAlO samples.

shown in Fig. 9, CO_2 was formed in the absence of gas phase O_2 for all samples, which can be assigned to the reactivity of surface active oxygen species. The amount of CO_2 produced are 921.6, 885.9 and 405.2 μmol/g for the 8K/MgAlO, 5K/MgAlO and 0K/MgAlO samples, respectively. This sequence is consistent with the result of CO-TPR. However, above ~600 °C, the formation of CO substituted for CO_2 should be attributed to strongly bonded lattice oxygen [41]. Because the 8K/MgAlO and 5K/MgAlO samples produced more CO in comparison with the 0K/MgAlO sample, the mobility of lattice oxygen also unambiguously increased after K addition. As the supported catalysts can be expected, the kind of lattice oxygen was limited to a surface K-containing layer.

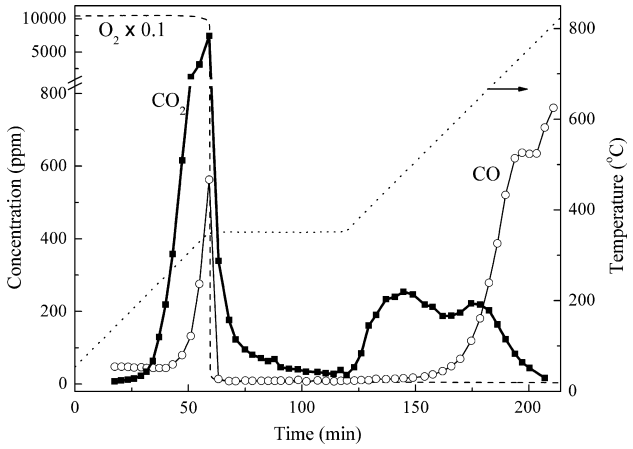

Fig. 10. Concentrations of CO_2, CO and O_2 as well as temperatures in the transient reaction on the 8K/MgAlO sample.

3.4. Transient reaction

In order to elucidate the reaction pathway, Fig. 10 shows a transient reaction over the 8K/MgAlO sample. In the 1st phase, soot was oxidized into CO_2 and CO while the temperature increased to 350 °C in the presence of O_2. When the dosage of O_2 was stopped at 350 °C in the 2nd phase, the CO concentration sharply dropped to zero, while the CO_2 concentration declined slowly, implying that some surface active oxygen on catalysts transferred to the ketene group. As the evolution of CO_2 decreased to zero, the ketene group diminished, which can be shown from the vanishing of its characteristic peak at 2171 cm^{-1} in Fig. 8d. In the 3rd phase, the temperature continued to rise under inert atmosphere, which resulted in the rapid CO_2 desorption and formation of two overlapped peaks, similar to CO_2-TPD (Fig. 6a inset). This illustrates that the carbonates formed in soot combustion were stable and could not decompose in time. CO reappeared at higher temperature of ~600 °C, the concentration increasing with heating, consistent with carbothermal reduction results. As shown in the 1st phase, the production of CO during soot isothermal combustion depends strongly on the presence of gas phase O_2, thus it can be shown that CO byproduct comes from the direct oxidation of free carbon sites by gas phase O_2. When the production of CO_2 is increased, the more free carbon sites will be exposed, meaning the more CO will be produced.

4. Discussion

It is long known that Al_2O_3 [42] is a nonactive sample, and MgO [10] has a negligible effect on soot combustion. Their mixed oxide derived from hydrotalcite was found to be similar to the performance of MgO without effect from Al, which is easy to understand considering they are not reducible. However, the introduction of K

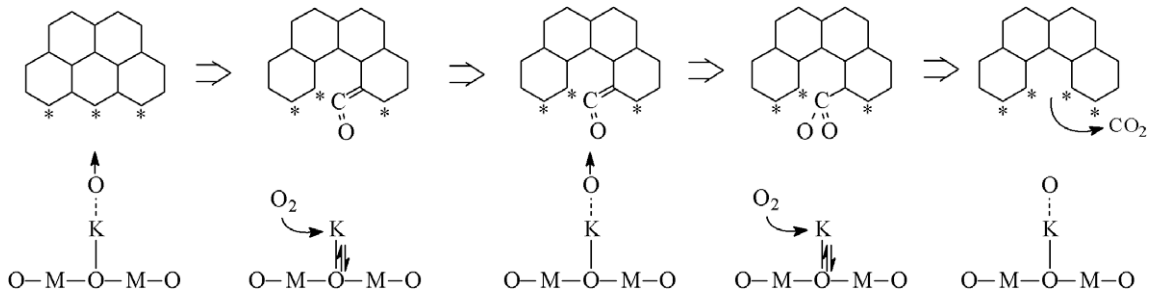

Fig. 11. Mechanism illustration of CO_x formation in soot combustion with O_2 on K-supported samples. M stands for metals of Mg or Al; C body is polyaromatic.

induced that the Al_2O_3, MgO and MgAlO samples are active. As shown in Table 1, in the first TPO reactions, T_m is in the sequence of: $8K/MgO \approx 8K/MgAlO \ll 8K/Al_2O_3$. On the other hand, all of the three samples suffer the degradation after repeated TPO cycles. Take the 20 times TPO cycles as examples, T_m (tight contact) rose about 12%, 7% and 19% for $8K/Al_2O_3$, 8K/MgAlO and 8K/MgO, respectively, corresponding to the loss ratios of K about 26%, 22% and 64% (detected by XRF). These facts suggest that although 8K/MgO possesses good activity, its stability is low due to the great loss of K. Contrarily, $8K/Al_2O_3$ shows low activity, but its stability is good. On the basis of XRD results (results not shown here), the loss of K for 8K/MgO is attributed to the vanishing of the bulk K_2CO_3 phase after 20 times TPO cycles. While in $8K/Al_2O_3$, the bulk $K_2Al_2O_4$ phase was formed, which means the incorporation of K into the catalyst. As given in Section 3.2, 8K/MgAlO shows neither K_2CO_3 nor $K_2Al_2O_4$ phases, then what is the intrinsic mechanism for both the high activity and stability?

There are two factors that affect the solid–solid–gas reaction system of catalytic soot combustion. One is the intrinsic oxidation capability of the catalyst itself, which is related to the redox mechanism (Mars and van Krevelen); the other is the contact condition between soot and catalyst, which is often associated with oxygen spillover [43,44]. In real situations, however, the contact is poor or loose. Therefore, the latter seems to be more important, in which the formation of a carbon–oxygen complex is a reaction intermediate step. Molecular orbital calculations have shown that the carbon–oxygen complex can substantially weaken surface C–C bonds in soot structure, leading to CO_x release [45].

First of all, as the K amount increases, the BET surface areas and pore volumes are inversely related to catalytic performance. Moreover, although the pore size increases, it is not accessible for the penetration of the soot agglomerates (size in about 177 nm) into catalyst pores (less than 100 nm), even in the tight contact mode [46]. Therefore, the contact between soot and catalyst in this work was not affected by the textural properties of catalysts. Secondly, DSC results do not show the occurrence of phase transition (results not shown here). Thus, the wetting of the soot surface through the low melting point compounds, or eutectics with other components of catalysts, was not expected in the temperature range of soot combustion [9]. Thirdly, the first H_2-TPR spectrum for the 8K/MgAlO sample shows only one H_2 consumption peak at about 690 °C, which corresponds to the reduction of surface carbonates into CO and H_2O [8] (results not shown here). However, the second H_2-TPR spectrum shows no peaks at any temperatures. Therefore, the presence of K does not modify the nonreducible characteristics of the mixed oxides derived from hydrotalcite, which ruled out the possibility of redox involving supports. Lastly, as displayed from *in situ* DRIFTS analyses, CO_2 appears at lower temperatures prior to the appearance of carbonate species. This fact conflicts with the results of a similar experiment [28], in which carbonate intermediate was first formed and decomposed to CO_2 at much lower temperature. Furthermore, in the temperature range of soot combustion from about 350–450 °C, the CO_2 desorption is not dominant as shown in CO_2-TPD. Accordingly, it is deduced that the combustion product CO_2 is released from a weakly adsorbed CO_x species.

A number of studies [4,19,47] have suggested that the carbon–oxygen complexes were formed during soot combustion. Specially, the carboxyl groups were identified by Liu et al. using an *in situ* UV-Raman spectroscopy [4]. In this work, the carbon–oxygen complex was identified to be the ketene group by an *ex situ* FTIR technique. As the intermediate, the ketene group vanished after reactions (Fig. 8d). In addition, the formation of the ketene group can be attributed to the transfer of oxygen species on K sites to the free carbon sites on soot. We have concluded these oxygen species were surface-activated oxygen and can be supplied by gas phase O_2 and surface lattice oxygen as indicated by XPS analysis and carbothermal reduction.

Taking into account the results discussed above, the reaction mechanism of K-supported Mg–Al hydrotalcite mixed oxides for catalytic combustion of soot is described in Fig. 11. All characterization results show that surface K species (both K_I and K_{II}) were active sites. The surface-activated oxygen on K sites might spill over to the free carbon sites on soot to form a carbon–oxygen complex, i.e. a ketene group, the reaction intermediate. The consumed surface oxygen can be replenished by the chemisorption and dissociation of gas phase oxygen or surface lattice oxygen due to K effect. The participation of the surface lattice oxygen in soot combustion, in the absence of gas phase oxygen, is evident in XPS, carbothermic reduction and transient reaction. The ketene group is further oxidized into CO_2 by other active oxygen, resulting in more exposed free carbon sites. The free carbon species can be directly oxidized into CO by gas phase oxygen, which brings about the selectivity of soot combustion. As shown in Table 3, with the increase in K, the amount of active sites increase, which will occupy more free carbon sites, avoiding combination with gas phase O_2 into CO, resulting in little increase in CO_2 selectivity. More importantly, K facilitates oxygen spillover to soot via the formation of ketene species. Thus, the spillover oxygen from catalyst to soot might act as the spreading of catalysts or as a liquid phase wetting of soot, as if the catalysts possess mobility, which ameliorated loose contact activity of K-supported samples [44].

Because the weak CO_2 peak at 700–750 °C during TPO or CO-TPR is not accompanied by CO production or consumption, it should come from the decomposition of carbonates, which is confirmed by CO_2-TPD. Taking 8K/MgAlO20 as an example, the disappearance/decrease of CO_2 desorption peak at 700–750 °C in TPO and CO_2-TPD patterns might be correlated with the loss of free K, which results in the decrease in activity, especially in loose contact conditions [1]. As indicated earlier, K and Al can form $KAl(CO_3)(OH)$ during reactions, which decomposes into highly dispersed surface K bound to Al after calcinations at higher temperatures. The simultaneous leaching of Al was also supported by XPS. However, this tightly bound K species, different from the separate aluminate

phase for $8K/Al_2O_3$, are both active and stable. Therefore, the decrease in Mg/Al ratio in hydrotalcite, namely, the increase of Al amount, might reduce the rate of K loss. This rooting of K on catalyst is a contribution to soot combustion of Al addition into MgO to form a K-supported composite oxide via the hydrotalcite route [11].

5. Conclusions

The catalytic activity of Mg–Al hydrotalcite mixed oxides for soot combustion with O_2 was significantly improved by the addition of potassium. The optimum amount of potassium was below 8 wt.% of the supporting amount.

The reaction proceeds via an oxygen spillover mechanism. First, the surface-activated oxygen on potassium sites spill over to the free carbon sites on soot to form a carbon–oxygen complex, ketene group, which was identified as the reaction intermediate. Then the ketene group combined with another active oxygen species to give out CO_2. Thus, more amounts of free carbon sites were exposed, resulting in the depletion of soot. The byproduct CO of soot combustion with O_2 came from the reaction of free carbon sites and gas phase O_2. The spillover oxygen may have acted as the spreading of catalysts or as a liquid phase wetting of soot, which ameliorated loose contact activity.

Two kinds of highly dispersed potassium species, Mg(Al)–O–K (tightly bound to Mg or Al) and free (isolated) potassium, were formed on catalysts. As catalytically active species, they were shown to increase the reactivity and amount of surface active oxygen responsible for the formation of the ketene group. Although the free K species were easily lost after repeated thermal cycles, the stability of K can be greatly improved through the interaction with Al. This is a contribution to soot combustion of Al addition into MgO to form a K-supported composite oxide via the hydrotalcite route.

Acknowledgments

This work was supported by the 863 program of the Ministry of Science and Technology of the People's Republic of China (No. 2008AA06Z320), the National Natural Science Foundation of China (Nos. 20577015 and 20777028) and the Natural Science Foundation of Shandong Province (No. 2007ZRB01259).

References

[1] H. An, P.J. McGinn, Appl. Catal. B 62 (2006) 46.
[2] J. Oi Uchisawa, A. Obuchi, Z. Zhao, S. Kushiyama, Appl. Catal. B 18 (1998) 183.
[3] Q. Liang, X. Wu, D. Weng, H. Xu, Catal. Today 139 (2008) 113.
[4] J. Liu, Z. Zhao, P. Liang, C. Xu, A. Duan, G. Jiang, W. Lin, I.E. Wachs, Catal. Lett. 120 (2008) 148.
[5] Y. Teraoka, K. Nakano, W. Shangguan, S. Kagawa, Catal. Today 27 (1996) 107.
[6] D. Fino, N. Russo, G. Saracco, V. Specchia, J. Catal. 242 (2006) 38.
[7] R. Jiménez, X. García, T. López, A.L. Gordon, Fuel Process. Technol. 89 (2008) 1160.
[8] E. Aneggi, C. de Leitenburg, G. Dolcetti, A. Trovarelli, Catal. Today 136 (2008) 3.
[9] V. Serra, G. Saracco, C. Badini, V. Specchia, Appl. Catal. B 11 (1997) 329.
[10] E.E. Miró, F. Ravelli, M.A. Ulla, L.M. Cornaglia, C.A. Querini, Catal. Today 53 (1999) 631.
[11] R. Jiménez, X. García, C. Cellier, P. Ruiz, A.L. Gordon, Appl. Catal. A 297 (2006) 125.
[12] C. Janiak, R. Hoffmann, P. Sjovall, B. Kasemo, Langmuir 9 (1993) 3427.
[13] M.S. Gross, M.A. Ulla, C.A. Querini, Appl. Catal. A 360 (2009) 81.
[14] R. Kimura, J. Wakabayashi, S.P. Elangovan, M. Ogura, T. Okubo, J. Am. Chem. Soc. 130 (2008) 12844.
[15] G. Fornasari, R. Glöckler, M. Livi, A. Vaccari, Appl. Clay Sci. 29 (2005) 258.
[16] B.A. Silletti, R.T. Adams, S.M. Sigmon, A. Nikolopoulos, J.J. Spivey, H.H. Lamb, Catal. Today 114 (2006) 64.
[17] Z. Zhang, Z. Mou, P. Yu, Y. Zhang, X. Ni, Catal. Commun. 8 (2007) 1621.
[18] B.A.A.L. van Setten, M. Makkee, J.A. Moulijn, Catal. Rev. 43 (2001) 489.
[19] M.A. Peralta, V.G. Milt, L.M. Cornaglia, C.A. Querini, J. Catal. 242 (2006) 118.
[20] R. Jiménez, X. García, C. Cellier, P. Ruiz, A.L. Gordon, Appl. Catal. A 314 (2006) 81.
[21] P. Darcy, P. Da Costa, H. Mellottée, J.M. Trichard, G. Djéga-Mariadassou, Catal. Today 119 (2007) 252.
[22] Z.H. Zhu, G.Q. Lu, R.T. Yang, J. Catal. 192 (2000) 77.
[23] M.J. Illan-Gomez, A. Linares-Solano, L.R. Radovic, C. Salinas-Martinez de Lecea, Energy Fuel 9 (1995) 97.
[24] Y. Wang, X. Wei Han, A. Ji, L.Y. Shi, S. Hayashi, Microporous Mesoporous Mater. 77 (2005) 139.
[25] A. Iordan, M.I. Zaki, C. Kappenstein, J. Chem. Soc. Faraday Trans. 89 (1993) 2527.
[26] S.C. Lee, H.J. Chae, S.J. Lee, B.Y. Choi, C.K. Yi, J.B. Lee, C.K. Ryu, J.C. Kim, Environ. Sci. Technol. 42 (2008) 2736.
[27] Y. Wang, J.H. Zhu, W.Y. Huang, Phys. Chem. Chem. Phys. 3 (2001) 2537.
[28] I.C.L. Leocadio, S. Braun, M. Schmal, J. Catal. 223 (2004) 114.
[29] K.I. Hadjiivanov, G.N. Vayssilov, Adv. Catal. 47 (2002) 307.
[30] S.E. Collins, M.A. Baltanás, A.L. Bonivardi, J. Mol. Catal. A 281 (2008) 73.
[31] A. Iordan, M.I. Zaki, C. Kappenstein, Phys. Chem. Chem. Phys. 6 (2004) 2502.
[32] S. Walspurger, L. Boels, P.D. Cobden, G.D. Elzinga, W.G. Haije, R.W.v.d. Brink, ChemSusChem 1 (2008) 643.
[33] S.J. Palmer, R.L. Frost, T. Nguyen, Coord. Chem. Rev. 253 (2009) 250.
[34] H. Zeng, Z. Feng, X. Deng, Y. Li, Fuel 87 (2008) 3071.
[35] J.I. Di Cosimo, V.K. Díez, M. Xu, E. Iglesia, C.R. Apesteguía, J. Catal. 178 (1998) 499.
[36] M. Haneda, Y. Kintaichi, I. Nakamura, T. Fujitani, H. Hamada, J. Catal. 218 (2003) 405.
[37] D.G. Cantrell, L.J. Gillie, A.F. Lee, K. Wilson, Appl. Catal. A 287 (2005) 183.
[38] G. Carja, R. Nakamura, H. Niiyama, Appl. Catal. A 236 (2002) 91.
[39] B.D. Wagner, B.R. Arnold, G.S. Brown, J. Lusztyk, J. Am. Chem. Soc. 120 (1998) 1827.
[40] K. Kobayashi, S. Shinhara, M. Moriyama, T. Fujii, E. Horn, A. Yabe, N. Furukawa, Tetrahedron Lett. 40 (1999) 5211.
[41] G.I. Panov, K.A. Dubkov, E.V. Starokon, Catal. Today 117 (2006) 148.
[42] P.G. Harrison, I.K. Ball, W. Daniell, P. Lukinskas, M. Céspedes, E. Miró Eduardo, M.A. Ulla, Chem. Eng. J. 95 (2003) 47.
[43] G. Mul, F. Kapteijn, J.A. Moulijn, Appl. Catal. B 12 (1997) 33.
[44] G. Mul, F. Kapteijn, C. Doornkamp, J.A. Moulijn, J. Catal. 179 (1998) 258.
[45] H.Y. Huang, R.T. Yang, J. Catal. 185 (1999) 286.
[46] K. Krishna, A. Bueno-Lóez, M. Makkee, J.A. Moulijn, Appl. Catal. B 75 (2007) 189.
[47] A. Setiabudi, M. Makkee, J.A. Moulijn, Appl. Catal. B 50 (2004) 185.